

Seismic Damage-Cracking Analysis of Concrete Dams Affected by Alkali-Aggregate Reaction

J.W. Pan, F. Jin, Y.J. Xu & C.H. Zhang

State Key Laboratory of Hydrosience and Engineering, Tsinghua University, Beijing, 100084, China

Y.T. Feng

Civil and Computational Engineering Centre, College of Engineering, Swansea University, Swansea, SA2 8PP, UK



SUMMARY:

A chemo-damage model is presented to analyse the nonlinear seismic behaviour of AAR-affected concrete dams. The chemo-damage model is implemented by combining the plastic-damage model with the AAR kinetics, and can predict cracking of concrete with a chemical reaction evolution law. Fontana gravity dam, a well-known case in dam engineering history, is analysed using the proposed model. The simulated cracking pattern in the dam caused by the continuing AAR is in good agreement with the field observation. A seismic analysis of the severely cracked dam is then performed. It shows that a new crack appears and penetrates the upper portion of the dam. The seismic stability of the dam is significantly reduced due to the AAR-induced cracking and deterioration of concrete.

Keywords: concrete dams, alkali-aggregate reaction (AAR), earthquake, cracking

1. GENERAL INSTRUCTIONS

Alkali-aggregate reaction (AAR) is the most common chemical reaction in concrete. It will trigger a progressive damage over time, and give rise to a network of micro and macro cracking in concrete. The AAR produces permanent swelling and causes material deterioration in concrete dams. The degradation of the concrete may affect the stability of a dam, especially when cracks further propagate from the previously AAR-induced flaws when the dam is subjected to strong earthquakes. The interaction of the cracks may cause a possible failure of the dam. Therefore, it is necessary to consider the AAR-induced damage prior to a strong earthquake in the seismic safety evaluation of concrete dams.

A few macroscopic models have been developed for analyzing the structural expansion resulted from AAR, among which Charlwood's model (1992) is one of the most widely used approaches. Charlwood's model assumes that the AAR swells with a constant rate during the reaction process, and does not agree with the AAR kinetics obtained from the experimental tests. Although the model has the capacity of obtaining the final amount of expansion displacement of AAR-affected concrete dams, it cannot reproduce an accurate structural deformation process with reasonable stress fields especially when nonlinearity is considered. Subsequently, more advanced models that can account for both the AAR kinetics and the mechanical behaviour have been developed (Huang and Pietruszczak 1996, Ulm *et al.* 2000, Steffens *et al.* 2003). Among them, Ulm's model, which adopts the reaction kinetics based on the work of Larive (1998), is widely accepted (Saouma and Perotti 2006, Comi *et al.* 2009). These models are successfully used for the quantitative assessment of the AAR expansion in time and space of concrete structures. Many studies are reported to predict the expansion deformation during the AAR process of concrete dams and verify it by field measurements of the crest displacements. Relative few works, however, focus on the cracking pattern in dams due to AAR, which has a significant influence on the structural stability. Moreover, to the authors' knowledge there has been little research on the seismic safety assessment of AAR-induced cracked and deteriorated dams. A comprehensive review of the research on modeling of AAR can be referred to Pan *et al.* (2012).

In this paper, an efficient numerical modelling is developed for seismic analysis of nonlinear behavior of AAR-affected dams. A chemo-damage model is first presented, which combines the plastic-damage model with the AAR kinetics based on Ulm's model. Subsequently, the cracking pattern of the Fontana gravity dam suffering from AAR are analysed by the proposed model, followed by the seismic analysis of the cracked and deteriorated dam.

2. MODELING METHOD

2.1. Chemo-Damage Model

In the elasto-plastic model of concrete involving the AAR effects, the total strain $\boldsymbol{\varepsilon}$ is defined as a sum of the elastic strain $\boldsymbol{\varepsilon}^e$, the plastic strain $\boldsymbol{\varepsilon}^{pl}$, the thermal strain $\boldsymbol{\varepsilon}^{th}$, and the strain due to AAR $\boldsymbol{\varepsilon}^{aar}$:

$$\boldsymbol{\varepsilon} = \boldsymbol{\varepsilon}^e + \boldsymbol{\varepsilon}^{pl} + \boldsymbol{\varepsilon}^{th} + \boldsymbol{\varepsilon}^{aar} \quad (2.1)$$

with

$$\boldsymbol{\varepsilon}^{th} = \alpha(T - T_{ini})\mathbf{m}; \quad \boldsymbol{\varepsilon}^{aar} = \frac{1}{3}\xi(t, T)\varepsilon_v^\infty\mathbf{m} \quad (2.2)$$

where α is the coefficient of thermal expansion; T is the current temperature; T_{ini} is the initial temperature; $\mathbf{m}^T = \{1, 1, 1, 0, 0, 0\}$ is a vector; ε_v^∞ is the material constant that specifies the maximal volumetric expansion strain induced by AAR in the stress-free experiment, and its magnitude depends on the chemical conditions; and $\xi(t, T)$ is the reaction extent related to the actual physical time t and the temperature T . The AAR strain calculated from Eqn. (2.2) is based on the hypothesis of isotropic swelling in concrete due to expansive gels produced by AAR.

The damage theory is introduced to the elastic-plastic model for describing the strain-softening behaviour of concrete. The state of the material, in terms of stiffness, depends on a scalar variable d , the so-called damage factor. The damage factor varies between 0 and 1, corresponding to a sound concrete and a fully damaged concrete, respectively. Following the isotropic damage model, the relation between the apparent stress $\boldsymbol{\sigma}$, the effective stress $\bar{\boldsymbol{\sigma}}$ and the damage factor d can be written by:

$$\boldsymbol{\sigma} = (1 - d)\bar{\boldsymbol{\sigma}} \quad (2.3)$$

with

$$\bar{\boldsymbol{\sigma}} = \mathbf{D}_0^e(\boldsymbol{\varepsilon} - \boldsymbol{\varepsilon}^{pl} - \boldsymbol{\varepsilon}^{th} - \boldsymbol{\varepsilon}^{aar}) \quad (2.4)$$

where \mathbf{D}_0^e is the initial elastic stiffness tensor of the material. The total damage of the material involves a mechanical damage induced by external loads and an AAR damage caused by expansive silica gels. Thus the damage factor is defined as follows:

$$d = 1 - (1 - d_{aar})(1 - d_m) \quad (2.5)$$

where d_m is the mechanical damage factor, and d_{aar} is the AAR damage factor.

The yield function of concrete is introduced, and the plastic strain rates is defined as follows

$$F(\bar{\sigma}, \boldsymbol{\varepsilon}^{\text{pl}}) = 0; \quad \dot{\boldsymbol{\varepsilon}}^{\text{pl}} = \lambda \frac{\partial Q(\bar{\sigma})}{\partial \bar{\sigma}} \quad (2.6)$$

where λ is the plastic multiplier, and $Q(\bar{\sigma})$ is the plastic potential.

The mechanical damage factor is determined by the effective stress and the plastic strain, and has the form:

$$d_m = d_m(\bar{\sigma}, \boldsymbol{\varepsilon}^{\text{pl}}) \quad (2.7)$$

The chemo-damage model is then implemented following the framework of the plastic-damage model. The details can be found in the references (Lee and Fenves 1998, Pan *et al.* 2009 and 2011).

2.2. AAR kinetics

The AAR expansion in time is governed by the rate of the chemical reaction, which significantly depends on the reactive temperature. The expansion evolution developed by Larive (1998) is adopted here, and the AAR extent has the following form:

$$\xi(t, T) = \frac{1 - e^{-\frac{t}{\tau_c(T)}}}{1 + e^{-\frac{t - \tau_L(T)}{\tau_c(T)}}} \quad (2.8)$$

where τ_c and τ_L are the characteristic time and the latency time of AAR expansion, respectively. The AAR extent ξ evolves from 0 (the start of AAR) and 1 (the completion of AAR). Figure 2.1 shows the evolution of ξ in time and the definition of the corresponding time constants τ_c and τ_L .

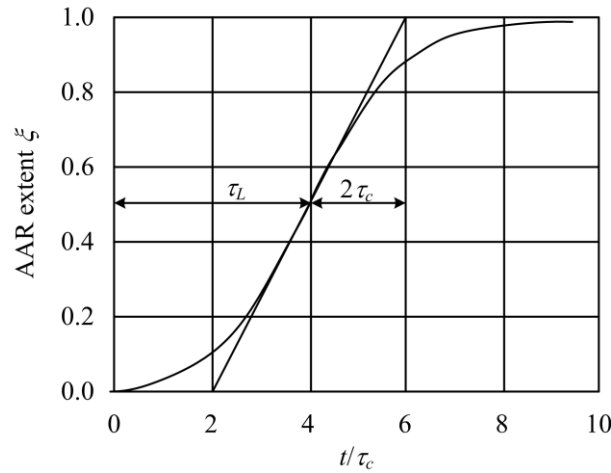


Figure 2.1. Evolution of the AAR extent ξ and definition of the latency and characteristic time τ_L and τ_c

The time constants are determined based on the Arrhenius relation from the stress-free swelling tests conducted by Ulm *et al.* (2000):

$$\tau_c(T) = \tau_c(T_0) e^{u_c \left(\frac{1}{T} - \frac{1}{T_0} \right)}; \quad \tau_L(T) = \tau_L(T_0) e^{u_L \left(\frac{1}{T} - \frac{1}{T_0} \right)} \quad (2.9)$$

where T_0 is the temperature at which the tests are carried out; U_c and U_L are the activation energies of the characteristic time τ_c and the latency time τ_L , respectively. The activation energy represents a threshold energy, or the minimum energy required to trigger the chemical reaction. The values of the activation energies are taken as:

$$U_c = 5400 \pm 500 \text{ K}; \quad U_L = 9400 \pm 500 \text{ K} \quad (2.10)$$

During the AAR process, the expansive gels destroy the concrete matrix and induce cracking of the aggregates and the surrounding cement paste. The damage of the material exhibits the degradation of mechanical properties, such as elastic stiffness, in the macroscopic behaviour of concrete. It is possible to link the AAR damage factor d_{aar} with the expansion strains based on the experimental results (Larive 1998, ISE 1992). The following equation is used to fit the experimental data:

$$\frac{E}{E_0} = \frac{B}{\varepsilon_A + B} \quad (2.11)$$

where E_0 and E are the initial and current Young's modulus, respectively; ε_A is the uniaxial strain induced by AAR; B is the fitting coefficient and taken as 0.003 (Capra and Sellier 2000). Therefore, the AAR damage factor in terms of expansion strain is obtained:

$$d_{\text{aar}} = 1 - \frac{E}{E_0} = \frac{\varepsilon_A}{\varepsilon_A + B} \quad (2.12)$$

Figure 2.2 presents the stiffness degradation of concrete in accordance with the AAR expansion strain and the corresponding fitted curve, together with the evolution of the AAR damage.

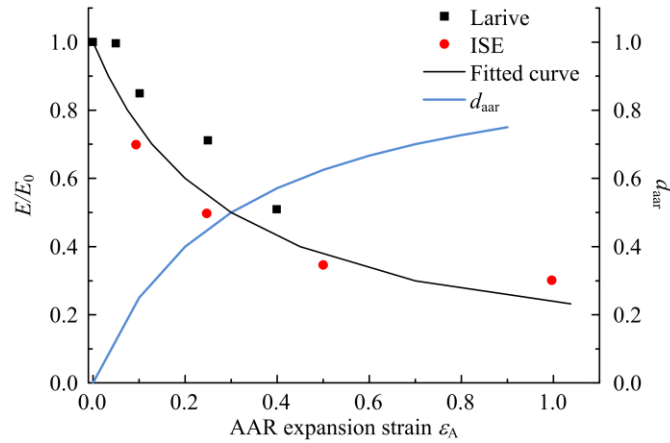


Figure 2.2. Stiffness degradation and AAR-induced damage over expansion strain

3. ANALYSIS OF FONTANA DAM

Fontana Dam is a well-known case in the dam engineering history due to the AAR-induced cracking in the dam. The Dam, completed in the winter of 1944, is located on the Little Tennessee River in North Carolina, United States. It is a concrete gravity dam with a maximum height of 147 m and length of 720 m. Only after 4 years of completion, networked cracks were observed in the parapets,

and continued extending over years. An increasing upstream deflection of the structure was also detected with plumb lines. Cracking was found in the walls of the foundation drainage gallery inside the dam near the left abutment during the structural inspection in 1972. The cracking extended from the gallery to the downstream face and a short distance upstream, as shown in Figure 3.1. The petrographic examination found deposits of alkali-silica gels and micro-cracks in the aggregates, revealing that AAR had occurred in the dam. A series of remedial measures has been performed to slow down the AAR development and strengthen the structure. Spraying cold reservoir water onto the downstream face of the dam to lower the temperature was conducted as an interim measure. Posttensioning the cracked blocks and grouting the cracks were later carried out. Finally, wide expansion slots across the upper portion of the dam, which interrupt the longitudinal thrust, were cut to release stresses in the dam caused by AAR (Newell and Wagner 1999).

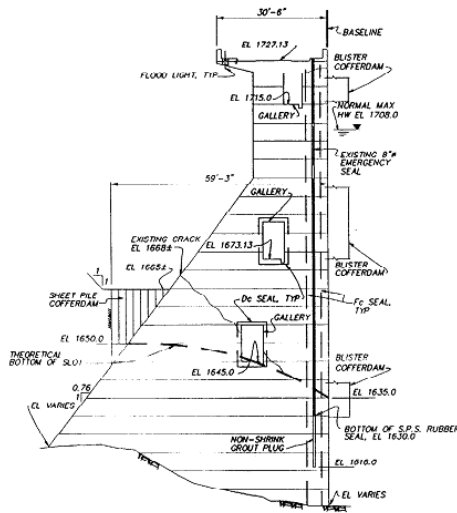


Figure 3.1. AAR-induced crack distribution in the Block 35 in Fontana Dam (Newell and Wagner 1999)

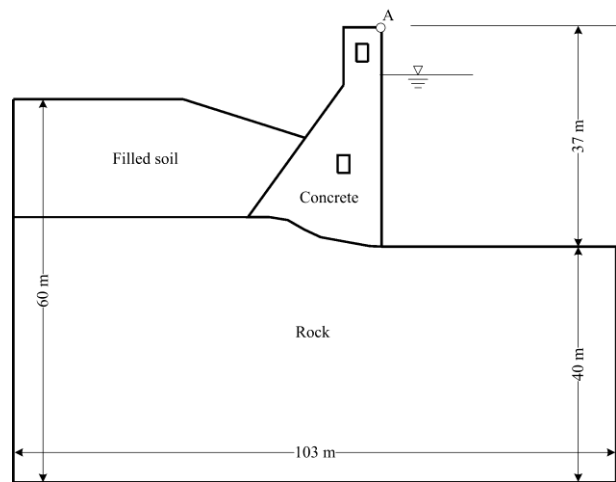


Figure 3.2. Geometry of the dam-foundation system

The cracking pattern of Fontana Dam caused by AAR is predicted using the proposed model, and then followed by a seismic analysis. The geometry of the entire dam is not available, thus a 2-meter-thickness slice of Block 35 of the dam is analysed. The geometry of the dam-foundation system is shown in Figure 3.2. The downstream filled-soil is considered in the model for possibly realistic boundary conditions of the dam during operation. Figure 3.3 presents the finite element (FE) discretization of the dam-foundation system. One layer of three-dimensional 8-node-brick elements is used across the thickness. Over the cross section, the mesh surrounding the galleries is refined with an element size of $0.2 \times 0.2 \text{ m}^2$ and is coarser in the other regions of the dam with the size of $0.4 \times 0.4 \text{ m}^2$. The mesh size in the foundation varies gradually from $0.4 \times 0.4 \text{ m}^2$ in the near field to $4.0 \times 4.0 \text{ m}^2$ in the far field.

The interactions between the dam and the foundation are considered using the contact boundary model (Bathe and Chaudhary 1985). The friction coefficient between the contact surfaces is taken as $\mu = 0.8$.

The mechanical and thermal properties of the materials are listed in Table 3.1. The foundation rock and the downstream filled-soil are assumed as linear elastic in the analysis. The AAR kinetics parameters, including the latency time, the characteristic time and the maximal volumetric expansion strain, are selected as $\tau_L(T_0) = 120$ days, $\tau_c(T_0) = 70$ days and $\varepsilon_v^\infty = 0.003$.

A transient thermal analysis of the dam-foundation system is first performed to determine the varying temperature field in the dam during the AAR process. The temperature field is then applied to account for the AAR kinetics and thermal stress in the proposed model. The air temperature, the reservoir level and the water temperature are required to impose proper boundary conditions in the thermal analysis.

The yearly variations of the air and water temperatures, together with the reservoir water depth, are given in Figure 3.4.

Following the transient thermal analysis, a mechanical simulation is performed. The gravity load of the dam is first applied, followed by the yearly varying hydrostatic pressure and the temperature load. The selected incremental time step is 2 days, and a duration of 20 years is analysed in both the thermal analysis and the mechanical simulation.

After the 20-year AAR swelling analysis, the strong 1967 Koyna earthquake, of which the recorded acceleration histories are shown in Figure 3.5, is applied to shake the AAR damaged dam. The horizontal and vertical peak ground accelerations of the earthquake are 0.47 g and 0.31 g, respectively. The massless foundation model is used. The dam–reservoir dynamic interactions are modelled according to the Westergaard added mass technique. The incremental time step is selected as 0.01 seconds in the seismic analysis.

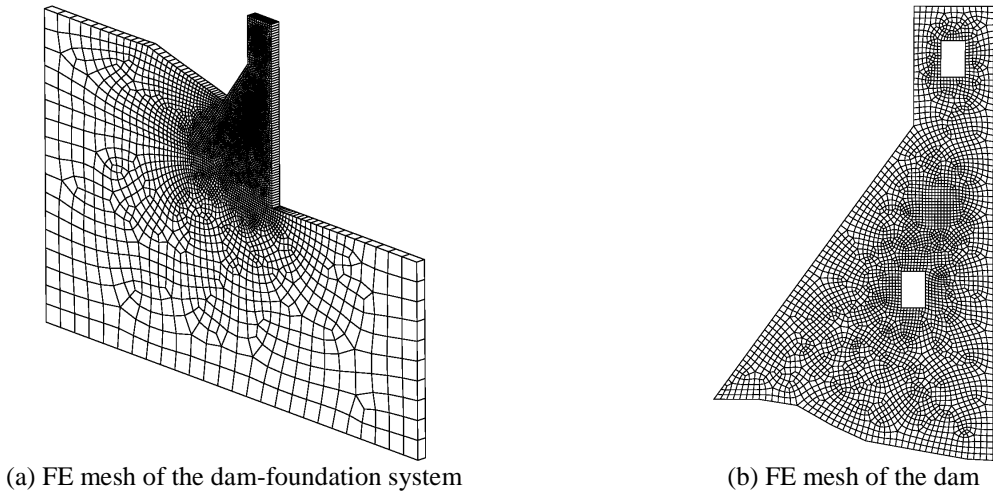


Figure 3.3. FE mesh of Block 35 in Fontana Dam

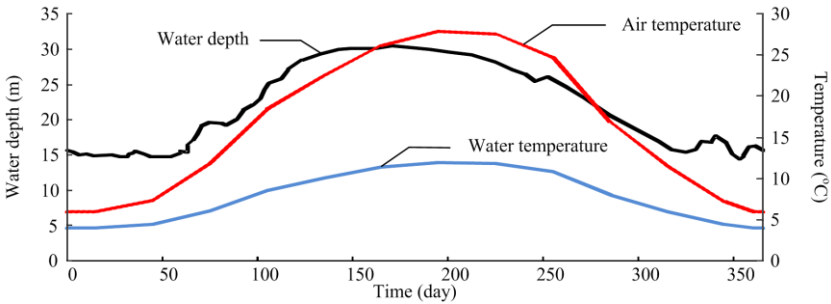


Figure 3.4. Yearly variation of pool water depth and temperature of water and air

Table 3.1. Material Properties of the Dam-Foundation System

	Young's Modulus	Poisson ratio	Tensile strength	Fracture energy	Thermal conductivity	Specific heat	Thermal expansion coefficient
	E_0	ν	f_t	G_f	k	c	α
	(GPa)	-	(MPa)	(N/m)	(W/(m K))	(kJ/(kg K))	(10^{-5})
Concrete	22.0	0.17	2.1	200.0	1.75	0.75	1.0
Rock	20.0	0.25	—	—	0.70	0.85	0.5
Filled-soil	0.15	0.2	—	—	0.55	1.00	0.5

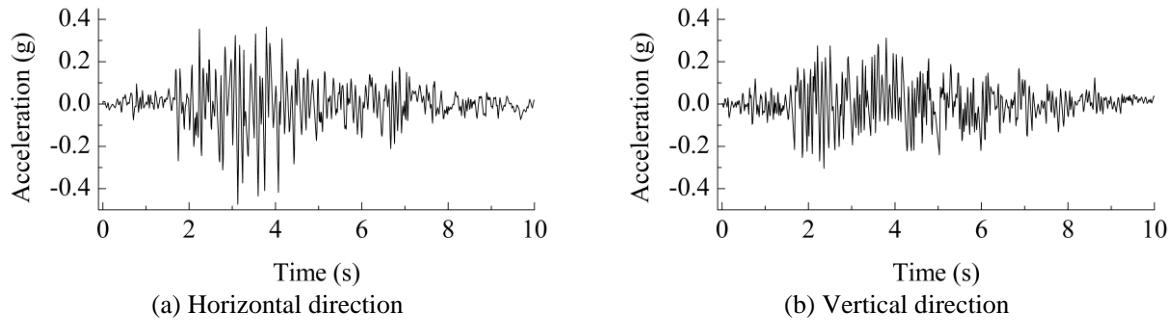


Figure 3.5. Input earthquake acceleration histories for the seismic analysis

Figure 3.6 presents the cracking propagation and damage pattern of the dam during the AAR process. Cracking initially occurs in the walls of the foundation drainage gallery inside the dam after $t=4$ years. The crack extends diagonally upwards towards the downstream face, where a new crack appears at $t=5$ years. These cracks form an inclined plane intersecting the section between the gallery and the downstream face after $t=13$ years. Another crack propagates a short distance upstream from the gallery. The predicted cracking pattern is in good agreement with the field observation. On the other hand, the concrete in the upper portion of the dam severely deteriorates after $t=20$ years.

The yearly variation of the crest displacements of the dam induced by the AAR expansion is shown in Figure 3.7. The horizontal crest displacement rapidly increases to its peak value of 2.6 cm at $t=6$ years, and decreases gradually until it reaches a permanent displacement of around 1.6 cm. The vertical crest displacement increases gradually and reaches its maximum value of 3.6 cm after 13 years.

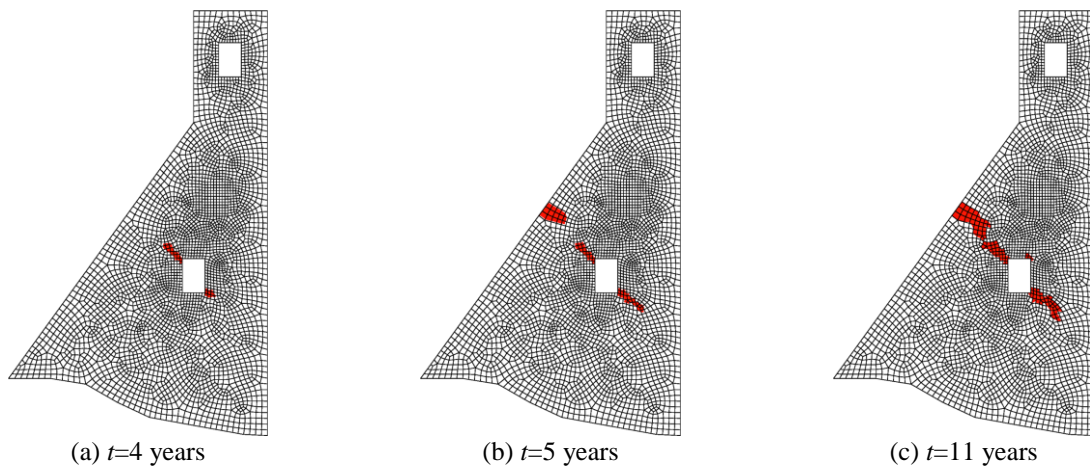


Figure 3.6. Cracking propagation and damage pattern in the dam during the AAR process

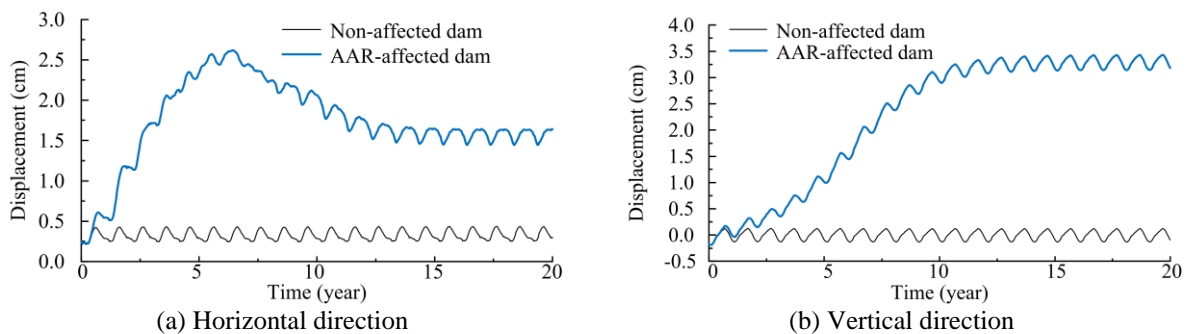


Figure 3.7. Yearly variation of crest displacement with time

Figures 3.8(a), (b) and (c) show the further cracking propagation of the cracked dam during the

earthquake. The AAR-induced cracks extend during the earlier stage of the seismic event, and stay stable afterwards. A new crack is formed at the upper portion near the slope change on the downstream face at about $t=2.5$ s. As the dam oscillates during the earthquake, the crack propagates deeper into the dam, and intersects with the upstream crack that initializes at $t=4.2$ s, thus penetrates the whole section of the dam. Some additional cracks are predicted to occur at the base of the dam. The seismic cracks are accompanied by the AAR-induced cracks, significantly reducing the safety of the dam. On the contrary, cracks that appear at the change of downstream slope and in the corners of the gallery only propagate a short distance into the non-affected dam after the seismic event, as shown in Figure 3.8(d).

The comparison of the crest displacements of the AAR-affected and non-affected dams subject to the earthquake is presented in Figure 3.9. There can be found a difference in the vibration periods, indicating that the vibration characteristic of the dam is significantly altered due to the cracking and damage of concrete caused by AAR. The maximum seismic displacements of the non-affected dam are 1.0 cm and 0.24 cm in the horizontal and vertical directions, respectively, while much larger maximum seismic displacements, 1.8 cm in the horizontal direction and 0.35 cm in the vertical direction, are obtained for the AAR-affected dam.

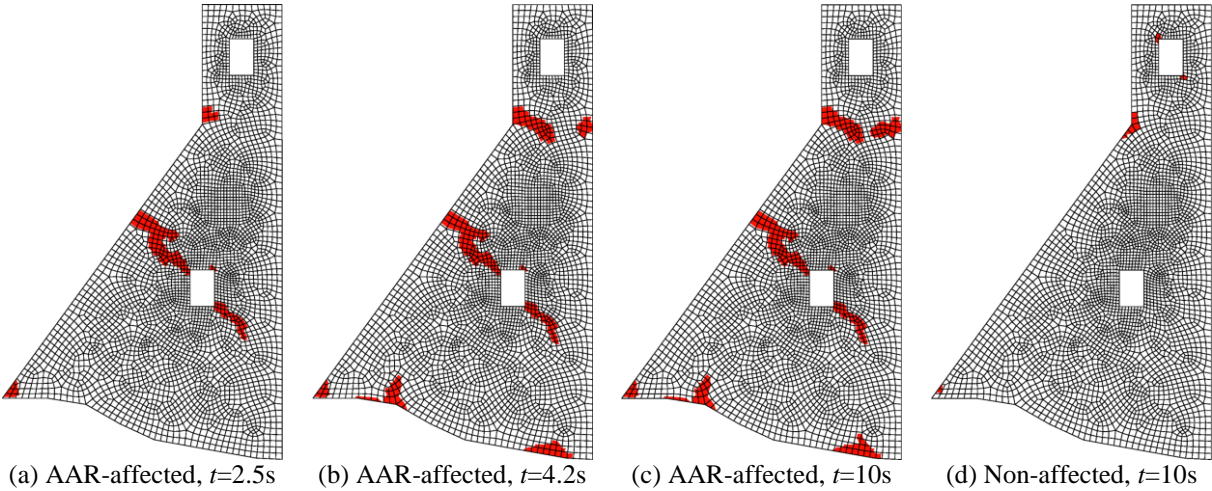


Figure 3.8. Cracking patterns of the AAR-affected and non-affected dam during the earthquake

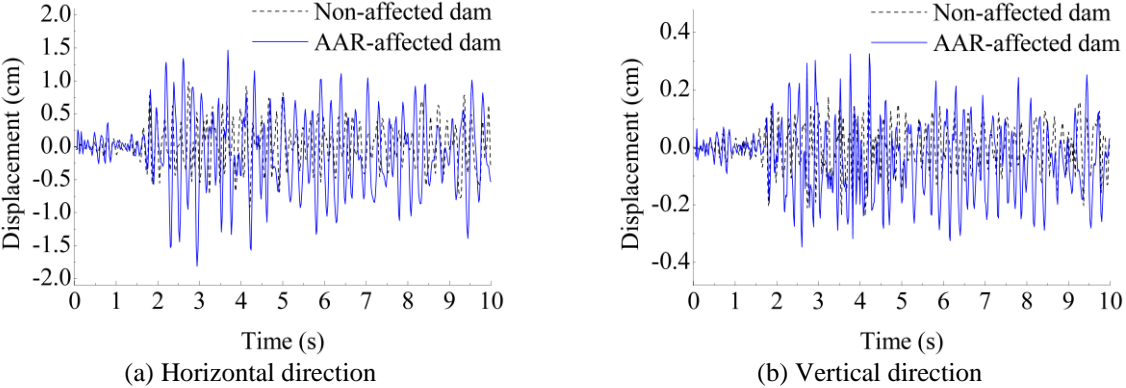


Figure 3.9. Seismic crest displacements of the dam

4. CONCLUSIONS

A chemo-damage model is presented to analyse the nonlinear behaviour of AAR-affected concrete

dams in the long-term operation condition and in the subsequent short-term seismic event. The chemo-damage model is implemented by combining the plastic-damage model with the AAR kinetics, which can predict cracking of concrete considering the reaction evolution law. Fontana gravity dam is analysed in the present work. The simulated cracking pattern in the dam induced by the continuing AAR is in good agreement with the field observation. The cracked and deteriorated dam is then shaken with a strong earthquake, and further cracking of the dam is observed. The seismic stability of the dam is significantly reduced due to the AAR-induced deterioration of concrete compared with the non-affected dam.

ACKNOWLEDGEMENT

The authors acknowledge the support for this research from the National Natural Science Foundation of China (Grant no.40974063).

REFERENCES

- Bathe K.J., Chaudhary A. (1985). A solution method for planar and axisymmetric contact problems. *International Journal for Numerical Methods in Engineering* **21**:1,65–88.
- Capra B., Sellier A. (2003). Orthotropic modelling of alkali-aggregate reaction in concrete structures: numerical simulations. *Mechanics of Materials* **35**:8,817-830.
- Charlwood R.G., Solyman S.V., Curtis D.D. (1992). A review of alkali aggregate reactions in hydroelectric plants and dams. *Proceedings of the International Conference of Alkali-Aggregate Reactions in Hydroelectric Plants and Dams, Fredericton, Canada*,**129**.
- Comi C., Fedele R., Perego U. (2009). A chemo-thermo-damage model for the analysis of concrete dams affected by alkali-silica reaction. *Mechanics of Materials* **41**:3,210-230.
- Huang M., Pietruszczak S. (1996). Numerical analysis of concrete structures subjected to alkali-aggregate reaction. *Mechanics of Cohesive-Frictional Materials* **1**:305-319.
- Institution of Structural Engineers.(1992). Structural effects of alkali-silica reaction, technical guidance on the appraisal of existing structures. SETO Limited, London.
- Larive C. (1998). Apports Combinés de l'Experimentation et de la Modélisation à la Compréhension del Alkali-Réaction et de ses Effets Mécaniques. *PhD thesis, Thèse de Doctorat, Laboratoire Central des Ponts et Chaussées, Paris (in France)*
- Lee J., Fenves L.G. (1998). Plastic-damage model for cyclic loading of concrete structures. *Journal of Engineering Mechanics ASCE* **124**:3,892-900.
- Newell V.A., Wagner C.D. (1999). Fontana Dam: a crack in the curve. *ASCE Conf Proc* **101**:25,1-10.
- Pan J.W., Feng Y.T., Wang J.T., Sun Q.C., Zhang C.H., Owen D.R.J. (2012). Modeling of alkali-silica reaction in concrete : a review. *Frontiers of Structural and Civil Engineering* **6**:1,1-18.
- Pan J.W., Zhang C.H., Wang J.T., Xu Y.J. (2009). Seismic damage-cracking analysis of arch dams using different earthquake input mechanisms. *Science in China Series E: Technological Sciences* **52**:2,518-529.
- Pan J.W., Zhang C.H., Xu Y.J., Jin F. (2011). A comparative study of the different procedures for seismic cracking analysis of concrete dams. *Soil Dynamics and Earthquake Engineering* **31**:11,1594-1606.
- Saouma V., Perotti L. (2006). Constitutive model for alkali-aggregate reactions. *ACI Materials Journal* **103**:3,194-202.
- Steffens A, Li K, Coussy O. (2003). Aging Approach to Water Effect on Alkali-Silica Reaction Degradation of Structures. *Journal of Engineering Mechanics of Materials ASCE* **129**:50-9.
- Ulm F.J., Coussy O., Li K., Larive C. (2000). Thermo-chemo-mechanics of ASR expansion in concrete structures. *Journal of Engineering Mechanics ASCE* **126**:3,233-242.